Geophysical Research Letters

RESEARCH LETTER
10.1029/2019GL082078

Seasonal Evolution of Oceanic Upper Layer Processes in the Northern Bay of Bengal Following a Single Argo Float

Abhijit Shee[1], Sourav Sil[1], Avijit Gangopadhyay[2,1], Glen Gawarkiewicz[3], and M. Ravichandran[4]

[1]School of Earth, Ocean and Climate Sciences, Indian Institute of Technology Bhubaneswar, Bhubaneswar, India, [2]School for Marine Science and Technology, University of Massachusetts Dartmouth, Dartmouth, MA, USA, [3]Woods Hole Oceanographic Institution, Woods Hole, MA, USA, [4]National Centre for Polar and Ocean Research, Goa, India

Key Points:
- Temperature inversion (~2.5 °C) in subsurface layer (30–110 m) is associated with thick barrier layer during winter due to deepening of ILD
- Subsurface temperature inversion diffuses in spring leading to thermal stratification and highest ML temperature
- In the northern BoB, the dominant forcing is thermal (haline) buoyancy during spring (fall) and wind during summer

Supporting Information:
- Texts S1-S4
- Figures S1-S5
- Movie S1
- Tables S1-S5

Correspondence to:
S. Sil,
souravsil@iitbbs.ac.in

Citation:
Shee, A., Sil, S., Gangopadhyay, A., Gawarkiewicz, G., & Ravichandran, M. (2019). Seasonal evolution of oceanic upper layer processes in the northern Bay of Bengal following a single Argo float. *Geophysical Research Letters*, *46*, 5369–5377. https://doi.org/10.1029/2019GL082078

Received 17 JAN 2019
Accepted 16 APR 2019
Accepted article online 24 APR 2019
Published online 21 MAY 2019

Abstract Seasonal evolution of the barrier layer (BL) and temperature inversion in the northern Bay of Bengal and their role on the mixed layer temperature (MLT) is examined using observations from a single Argo during December 2013 to July 2017. During fall, low salinity at surface generates BL in this region. It thickens to almost 80 m in winter enhanced by deepening of isothermal layer depth due to remote forcing. During winter, surface cooling lowers near-surface temperature, and thus, the subsurface BL experiences a significant temperature inversion (~2.5 °C). This temperature inversion diffuses to distribute heat within ML and surface heating begins deep penetration of shortwave radiation through ML during spring. Hence, the ML becomes thermally well stratified, resulting in the warmest MLT. The Monin-Obukhov length attains its highest value during summer indicating wind dominance in the ML. During spring and fall, upper ocean gains heat allowing buoyancy to dominate over wind mixing.

Plain Language Summary The northern Bay of Bengal is well known for its fresh ocean surface due to low salinity input from rivers. This study investigates the hydrography from the temperature and salinity profiles obtained from an Argo float, which drifted for 44 months in the northern Bay of Bengal. The mixed layer depends on the local processes and isothermal layer depth depends on the remote forcing through propagating Rossby waves. Thermal inversion within thick barrier layer is observed during winter. Wind stress is the dominant forcing in setting up the mixed layer during summer and winter. The barrier layer and temperature inversion play important roles on the mixed layer temperature. The state-of-the-art models failed to reproduce the temperature inversion layer due to low vertical resolution. While this is an integrated view from a single Argo, high-frequency high-resolution sampling would be necessary to understand turbulent mixed layer processes and quantify relative roles of haline buoyancy to thermal buoyancy.

1. Introduction

The variability of sea surface temperature (SST) in the Bay of Bengal (BoB) has been studied by several researchers through the mixed layer (ML) heat budget (MLHB) analysis, as SST is controlled by the ML dynamics, using both observations (Girishkumar et al., 2013; Parampil et al., 2010; Rao & Sivakumar, 2000; Sengupta & Ravichandran, 2001; Shenoi et al., 2002; Sengupta et al., 2002, hereafter GK13) and model (Montégut et al., 2007; Shaji et al., 2003). Vinayachandran and Shettye (1991) reported a large agreement between SST variability and the rate of heat storage of the top 50-m layer in the northern BoB. Wind also plays an important role on the ML temperature (MLT) evolution. In the BoB weaker winds are unable to overcome the strong near-surface stratification and thus cannot remove heat and salt from the upper ocean (Shenoi et al., 2002). This makes a stable shallow ML that quickly responds to atmospheric forcing. The combination of large lateral river inputs and precipitation makes the surface layer more buoyant and strongly stratified (Jana et al., 2015). The strong stratification forms a barrier layer (BL) between the base of the ML and the top of the isothermal layer (IL). Thus, the salinity stratification plays a crucial role in maintaining a high SST in winter and the presence of freshwater near the surface allows heat storage below the surface layer in the BoB (Montégut et al., 2007). The presence of a warm subsurface layer between the surface and subsurface colder waters means that temperature inversions occur within the BL (Thompson et al., 2006). The temperature inversions occur during winter when heating in the BL by penetrative shortwave

radiation is greater than the heating of the ML by the net surface heat flux and the horizontal advection (Girishkumar et al., 2011, hereafter GK11; GK13). The IL in the BoB also depends on the equatorial remote forcing in-terms of the coastally trapped Kelvin waves and radiated Rossby waves (RWs; Rao et al., 2010; (Yu et al., 1991; GK11; GK13; Kumari et al., 2018, hereafter KM18). Prasad (1997) and Anitha et al. (2008, hereafter AN08) used the Monin-Obukhov length (M-O length), which determines the relative importance of mechanical mixing (wind forcing) and surface buoyancy for analyzing stability and seasonality in the BoB.

While previous studies clearly indicate the importance of salinity stratification and temperature inversion for understanding the BL thickness (BLT) and ML dynamics (Thadathil et al., 2007; GK11; GK13; KM18), there are limited studies in the northern BoB. It is a data sparse region and highly stratified due to the presence of low salinity water. The Argo program has substantially increased the time series observations. We observed that an Argo float (WMO ID 5904302) is one of the very few long-term Argo floats in the BoB, which almost traveled the whole northern extent of the BoB (above 15°N) and provided temperature and salinity profiles in the northern BoB for depths up to 2,000 m for 44 months from December 2013 to July 2017 (Figures 1a–1d). This float offers a tremendous opportunity to use this long-term data for studying the upper and ML dynamics. The goal of the work is to answer the following questions (i) What is the seasonality of the MLHB in the northern BoB? (ii) What are the roles of the BL and inversion layer on the evolution of the MLT? And (iii) what is the contribution of surface buoyancy flux on the MLT in the northern BoB? The manuscript is arranged as follows: section 2 describes the material and methods, and section 3 presents key results followed by summary and conclusions in section 4.

2. Materials and Methods

2.1. Data

Temperature and salinity profiles from an Argo float (WMO ID: 5904302), which was deployed at a front near the region 16.5°N, 85.5°E on 21 November 2013, are used in this study. From 21 November to 8 December 2013 the float profiled rapidly from 0–250 m at 1.7-hr intervals (Johnston et al., 2016). From 9 December 2013, the float entered into the typical Argo mode to provide temperature and salinity profiles with 5-day interval and 1-m vertical resolution till 24 July 2017. The details of data availability and processing steps are provided in the supporting information (Text S1).

2.2. ML Depth

We calculate the ML depth (MLD) as the depth "h" at which the density ($\sigma_{t(z\,=\,h)}$) is equal to the surface value ($\sigma_{t(z\,=\,0)}$) plus an increment equivalent to the density change associated with some prescribed change in temperature (T; Kara et al., 2000; Millero et al., 1980; Rao & Shivakumar, 2003; Sprintall & Tomczak, 1992; Thadathil et al., 2007; Wyrtki, 1971). See Text S2 for definition of the MLD, IL depth (ILD), temperature inversions, and BLT.

2.3. MLHB Equation

The governing equation for the MLHB is as follows (Du et al., 2005; GK13; Montégut et al., 2007; Qu, 2003):

$$\frac{\partial T}{\partial t} = \frac{Q_{net} - Q_{pen}}{\rho C_p h} - \left[(u_g + u_{ek}) \frac{\partial T}{\partial x} + (v_g + v_{ek}) \frac{\partial T}{\partial y} \right] + H \left[W_e \frac{(T - Td)}{h} \right] + \frac{K_z}{h} \frac{\partial T}{\partial z} + \text{Residua} \qquad (1)$$

|__a_| |___b____| |_____c_____| |___d___| |__e__|

The individual terms are explained in Text S3.

2.4. Net Surface Buoyancy

The net surface buoyancy flux (NSBF) has two components, thermal buoyancy (B_T) and haline buoyancy (B_S), and is computed as (AN08; Prasad, 1997; Sutherland et al., 2013; Zhang & Talley, 1998)

$$B_0 = B_T + B_S = -g(\alpha F_T + \beta F_S) \qquad (2)$$

The terms are explained in Text S4.

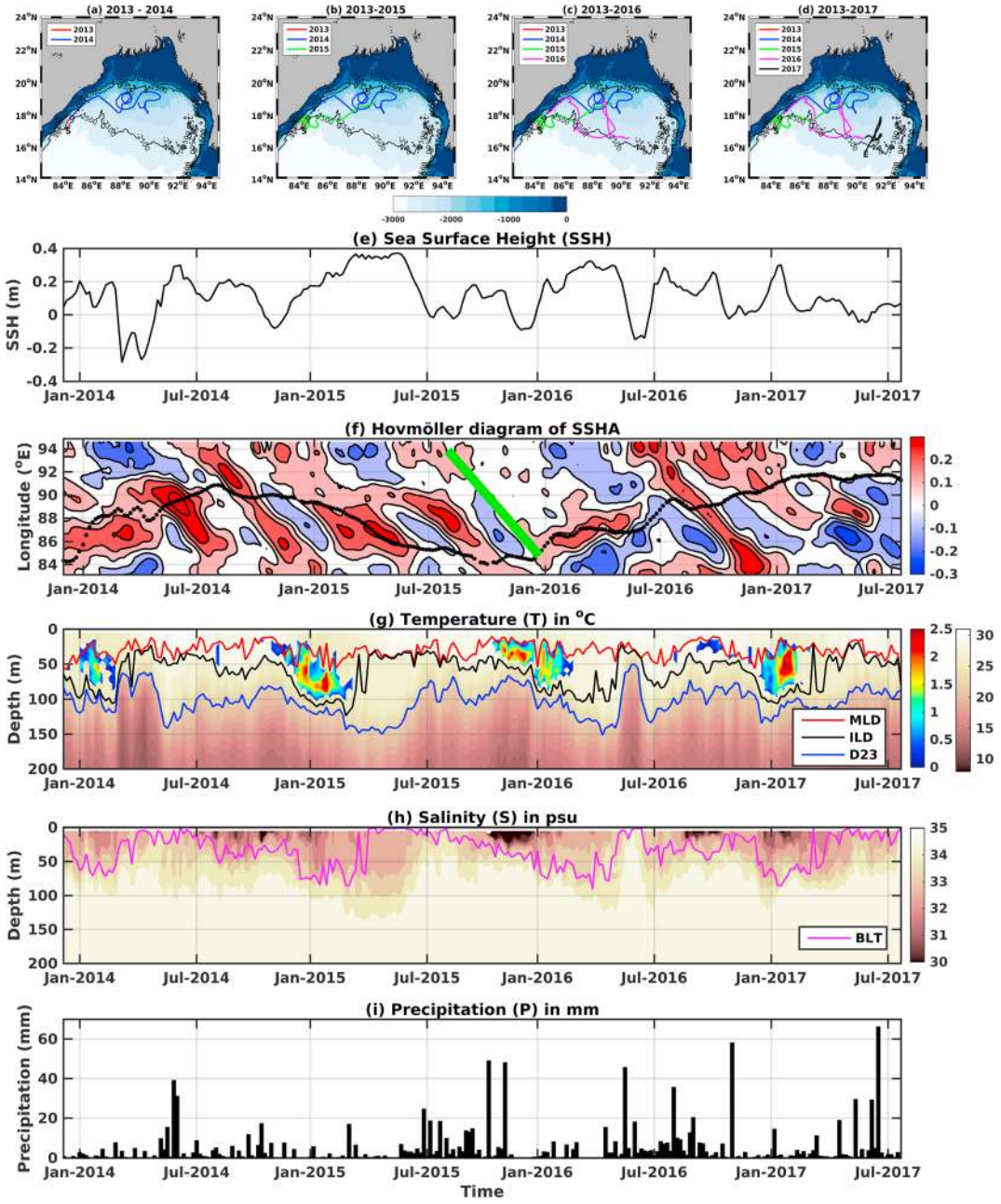

Figure 1. (a–d) Movements of the Argo float (WMO ID: 5904302) in different years from December 2013 to July 2017. S and E points indicate initial and endpoints of the trajectory. The background represents the domain bathymetry from ETOPO2 with contour lines of 1,500- and 2,500-m depths. (e) Time series of sea surface height anomaly (SSHA) along the float, (f) Hovmöller diagram of latitudinal averaged SSHA between 17°N to 19°N. Black dots represent the longitudinal positions of Argo. The green line indicates the absence of RW in 2015. Time depth section of (g) temperature and (h) salinity, and (i) temporal evolution of precipitation (bar plot) along the Argo float trajectory. Time depth section of temperature inversion are shown in Figure 1g using jet color map. Time series of MLD (red line), ILD (black line), and 23 °C isotherms (D23, blue line) are shown in (g), and BLT (magenta line) in (h). The ticks along the *x* axis represent the first day of the given month. MLD = mixed layer depth; ILD = isothermal layer depth; BLT = barrier layer thickness.

3. Results and Discussions

3.1. Float Trajectory

The Argo float starts at the western boundary region of the Bay on 9 December 2013 from 17.12°N, 85.36°E and ends its journey on 24 July 2017 at 16.73°N, 91.28°E in the eastern basin. The float drifted along different multiscale circulation features in the northern BoB for a duration of 44 month. Specifically, during most of

January-February-March of both 2014 and 2016, it traversed similar paths along the western Boundary Current and its associated anticyclonic eddy system. The float traveled along the edges of a series of cyclonic (March–April 2014; October–November 2014; November–December 2015; May–June 2016; and during October 2016 and May 2017) and anticyclonic (May–June 2014; January–June 2015; January–April 2016; June–September 2016; December 2016 to January 2017) eddies (Figures 1a–1d). These events are evident in their coincident SSH signatures in Figure 1e. The Hovmöller diagram of sea surface height anomaly (SSHA; Figure 1f) indicates the presence of westward propagating periodic downwelling (red) and upwelling (blue) RWs. Note that during January–June 2015, the Argo is within an anticyclonic eddy, which can be inferred from the positive SSHA in Figure 1e, which is also part of a downwelling RWs (Figure 1f). Similarly, during May–June 2016, it is in a cyclonic eddy associated with upwelling RWs. A dynamic visualization of the float trajectory is available online as an animated Movie S1.

3.2. Hydrography From Argo

Time-depth sections of temperature and salinity i.e., the thermohaline structure in the upper 200-m depth are shown in Figures 1g and 1h. Temporal evolution of MLD and ILD, and time-depth section of temperature inversions (using jet color map) are shown in Figure 1g. Temporal evolution of BLT and precipitation are shown in Figures 1h and 1i respectively. Strongest vertical temperature gradient occurs around the depth of the 23 °**C** isotherm (D23), which is covarying with the SSHA around the float (Figure 1e). The D23 is deeper (shallower) when SSHA is positive (negative; Figures 1e and 1g). Such variation can be interpreted as a combination of impact of RWs and local movements of the float within anticyclonic (cyclonic) eddies (Figure 1e). As they follow a seasonal cycle, the variations of the parameters are presented seasonally: (i) winter (December to February), (ii) spring (March–May), (iii) summer (June–September), and (iv) fall (October–November).

During the winter monsoon, ILD (black line, Figure 1g) increases to a maximum depth (~90–100 m) due to sea level variations by downwelling RWs (Figures 1e and 1f; Rao et al., 2010; Yu et al., 1991; Yu, 2003; GK11; KM18). Therefore, it shows the higher correlations with SSHA ($R = 0.64$) and D23 ($R = 0.74$), and negligible correlation ($R = 0.04$) with local wind stress (WS; Table S1). The low salinity is found to be distributed vertically to deep the MLD (Figure 1g). The variations of MLD (red line) and D23 (blue line) during winter are between 30–50 and 100–120 m, respectively (Figure 1g). The correlations of MLD with SSHA and D23 are less, which indicate that the MLD is not governed by the ocean dynamics and remote forcing. The MLD shows higher negative correlation with penetrating shortwave radiation (Q_{pen}) and positive correlation with the sea surface salinity (SSS). The difference between ILD and MLD forms a thick (>50 m) BL in the northern BoB. Relatively greater temperature inversions (maximum 2.5°**C** more than surface water) are observed within the BL in the winter monsoon, which is higher than that in southern BoB (~0.7°**C**) as was observed by GK13. Due to deepening of ILD, the warmer surface deepens to make subsurface warmer and the heat is trapped at the base of ML to form an inversion layer in winter (Figure S1).

The ILD, during spring, becomes very shallow (<50 m) due to upwelling RWs (Figures 1e and 1f), close to the variation of the MLD. Deep penetration of shortwave radiation through the ML helps to entrain the warm subsurface water from BL, which makes the BL very thin (0–20 m). The BLT is highly correlated with ILD and negligibly with MLD. The MLD is controlled by Q_{pen} only, which makes the layer thermally stratified (Table S2). The very low correlation with SSS indicates that less haline stratification exists in the northern bay during spring associated with higher salinity (Figure 1h). However, the D23 deepens (120–150 m) in the spring relative to winter except in March–April of 2014 (60 m) and May of 2016 (30 m). In these periods, the Argo moved along with a strong cyclonic (upwelling) eddy to reduce the D23 (Figure 1g) and can be observed from the associated negative SSHA (Figure 1e).

During the summer monsoon, the MLD becomes shallower ~25 m due to Q_{pen} ($R = -0.78$) and low SSS ($R = 0.70$) because of huge precipitation (Figure 1i) and river discharge (Table S3). The ILD deepens slightly to vary between 40 and 50 m due to downwelling RWs (Thadathil et al., 2007). Hence, BLT again increases and varies between 10 and 20 m (magenta line; Figure 1h), which depends both on ILD and MLD. Normally, in August, relatively weaker temperature inversions (~0.5 °**C**) are observed in the northern BoB (Figure 1g) similar to the southern BoB (GK13). But this is absent in 2015 (green line; Figure 1g), which is a positive IOD (India Ocean Dipole) year (http://www.bom.gov.au/climate/iod/) when the equatorial remote forcing is generally weaker (KM18). Hence, the deepening of ILD is less in 2015 compared to negative IOD years

(2014 and 2016), which make BLT comparatively less and the temperature inversion is absent. The mean thermocline (D23) during summer varies within the range 90–100 m (Figure 1g).

After summer, ILD shows similar variation during the fall, but the MLD becomes shallowest among all seasons (5–20 m) due to increased Q_{pen} ($R = -0.76$), the weak northeasterly winds and presence of low saline water ($R = 0.68$) at the surface (Figure 1h; Table S3). Thus, BLT in this season is observed to vary within 15–40 m (Figure 1h) due to shoaling of MLD ($R = -0.69$). In this season, D23 is shallowest among all other seasons (62–85 m) due to upwelling RWs.

We also investigated such thermocline behavior in two model simulations: (i) a general circulation model HYCOM analysis and (ii) ORAS4 reanalysis (Balmaseda et al., 2012) (see Text S1). The HYCOM and ORAS4 have only 10 and 17 vertical levels respectively in the top 200 m, whereas, the Argo has 200 levels (1m resolution). Comparisons show that both models capture the seasonal variability of temperature and salinity (Figures S2 and S3). However, the temperature inversion is only captured in the ORAS4, but with comparably less magnitude (Figure S3, left panel). This suggests that the reanalysis product, which assimilates the observations, is closer to reality and is needed for the northern BoB. The models capture the ocean dynamics with reasonable correlation for ILD, BLT, and D23 (Figures S4 and S5). However, the ML dynamics is not captured adequately, poorer in HYCOM. These highlight the need for improving the parameterization of mixing scheme and atmospheric forcing and adding more vertical layers in the ocean models. In the following sections, the dynamics of the ML is analyzed through heat budget computation to quantify different processes controlling the MLT.

3.3. MLHB Analysis

The MLHB is determined by three factors: net surface heat flux, horizontal advection, and vertical processes. The temperature tendency of the surface layer is a result of the balance among these three factors (equation (1)). The MLT is highly correlated ($R = 0.96$) to the near-surface temperature (NST) at 5 m and has a root-mean-square difference of 0.07 **°C.** The MLT covaries with SST semiannually with primary (secondary) peak in May (October; Figure 2a). The NSHF (Figure 2b) depends on the loss of penetrative shortwave radiation (Q_{pen}, Paulson & Simpson, 1977) across the ML. The horizontal temperature advection (Figure 2c) due to surface currents represents an exchange between the ML and the interior regions of high MLD gradient. Vertical processes are the combination of entrainment mixing and vertical diffusion (Figure 2d). The seasonal variation temperature tendency (Figure 2e), NSHF (source: Praveen Kumar et al., 2012), and vertical processes in the northern BoB are clearly observed.

During the winter, the NSHF (Figure 2b) is negative (**-250 to -50 W/m^2**), leading to cooling, while vertical processes show a weak warming tendency (**$\geq$20 W/m^2**). The overall temperature tendency in winter results in low MLT (26**$-$27 ° C**) compared to other times of the year in the northern BoB (Figure 2a). However, the MLT is higher than the NST due to the presence of the warm subsurface (temperature inversion) associated with the BL. In the winter of 2015–2016, the MLT shows higher values than other years due to higher NSHF and reduced horizontal advection. This time (a positive IOD year) the inversion layer forms at relatively shallower depth with thinner BL (Figures 1g and 1h). During spring, net heat flux (NHF) increases to a maximum value of 180 **W/m^2**. The Q_{pen} also reaches a maximum (**~35 W/m^2**), and overall NSHF in this season shows a strong warming tendency. On the other hand, vertical processes during these months show a strong cooling tendency (**$\leq -$ 40 W/m^2**) and the horizontal advection has positive tendency. Therefore, overall temperature tendency during spring shows the heat gain and the MLT increases to **31 ° C** in May in the presence of very thin BL and absence of temperature inversion. Due to the presence of clouds during the summer, the net shortwave radiation decreases and the NSHF varies between (**-50 and 150 W/m^2**). Therefore, the MLT in summer cools down to ~29**°C**. During fall, the net shortwave radiation and Q_{pen} again increases. Weak contribution from the vertical advection and the horizontal advection makes the MLT increase (**~29.5 $-$ 30.5 ° C**) associated with moderate BLT. The cooling (warming) tendency is observed as the Argo passes through cyclonic (anticyclonic) eddies. The time series of the MLT tendency (black line; Figure 2e) and the sum of all processes (red line; Figure 2e) match closely.

3.4. Surface Buoyancy Flux

The balance between energy production and suppression by buoyancy and dissipation controls the amount of turbulent kinetic energy in the ocean and is significant for mixing (Sutherland et al., 2013). The buoyancy

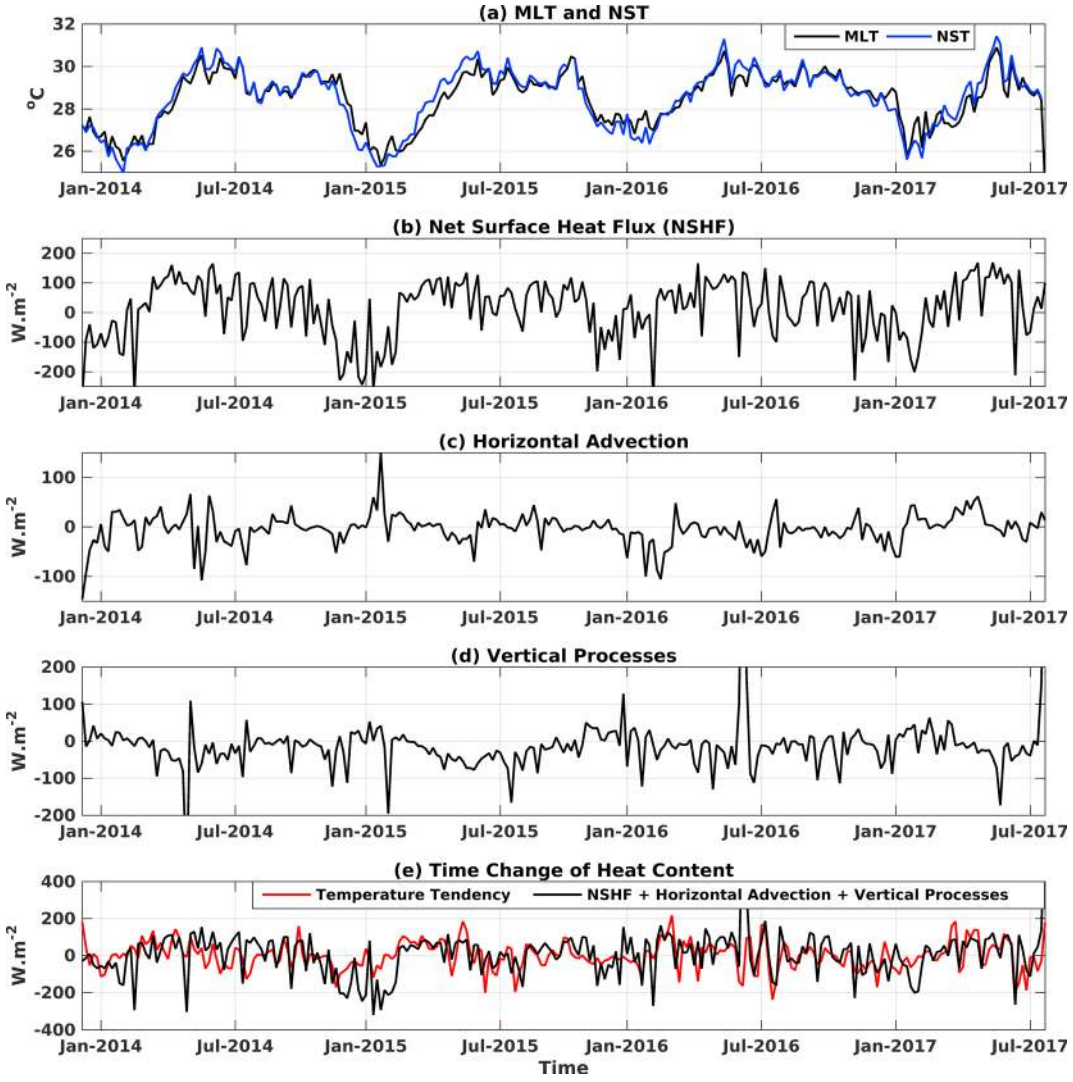

Figure 2. Time series of (a) MLT and NST, (b) net surface heat flux (NSHF), (c) horizontal advection, (d) vertical processes, and (e) temperature tendency (red line) along the float trajectory. The sum of NSHF, horizontal advection, and vertical processes are shown in (e) with black line. MLT = mixed layer temperature; NST = near-surface temperature.

forcing is exemplified as the change in surface density through the radiative (changing temperature) and hydrological (precipitation and evaporation) forces (changing salinity). The surface buoyancy has two components: thermal buoyancy ($\boldsymbol{B_T}$) and haline buoyancy ($\boldsymbol{B_S}$); see section 2.3.

Both surface warming and precipitation make the ocean surface more buoyant and provides stable conditions (AN08). Conversely, surface cooling through heat loss by the ocean or evaporation makes ocean surface less buoyant, which increases the surface density and creates unstable conditions. Hence, the surface buoyancy flux has an important role in determining the stability of the upper ocean and controlling the MLT. The thermal buoyancy flux (Figure 3a) is dominated by the NHF (Figure 2b) with positive values during spring and summer with a maximum in spring ($\sim 1.5 \times 10^{-7}\ \mathrm{m^2/s^3}$). In fall, the thermal buoyancy shifts from positive to negative values (Figure 3a). In winter, it is negative, which leads to cooling of MLT. The haline or freshwater buoyancy flux is positive throughout the study period and the range of variation is almost 10 times that of the thermal buoyancy (Figures 3a–3c). During summer and fall, higher precipitation (Figure 1i) decreases the surface salinity (Figure 1h) and increases the haline buoyancy to its maximum ($4 \times 10^{-6}\ \mathrm{m^2/s^3}$). The NSBF is dominated by the haline buoyancy flux, which reaches large values during summer and fall (Figure 3c).

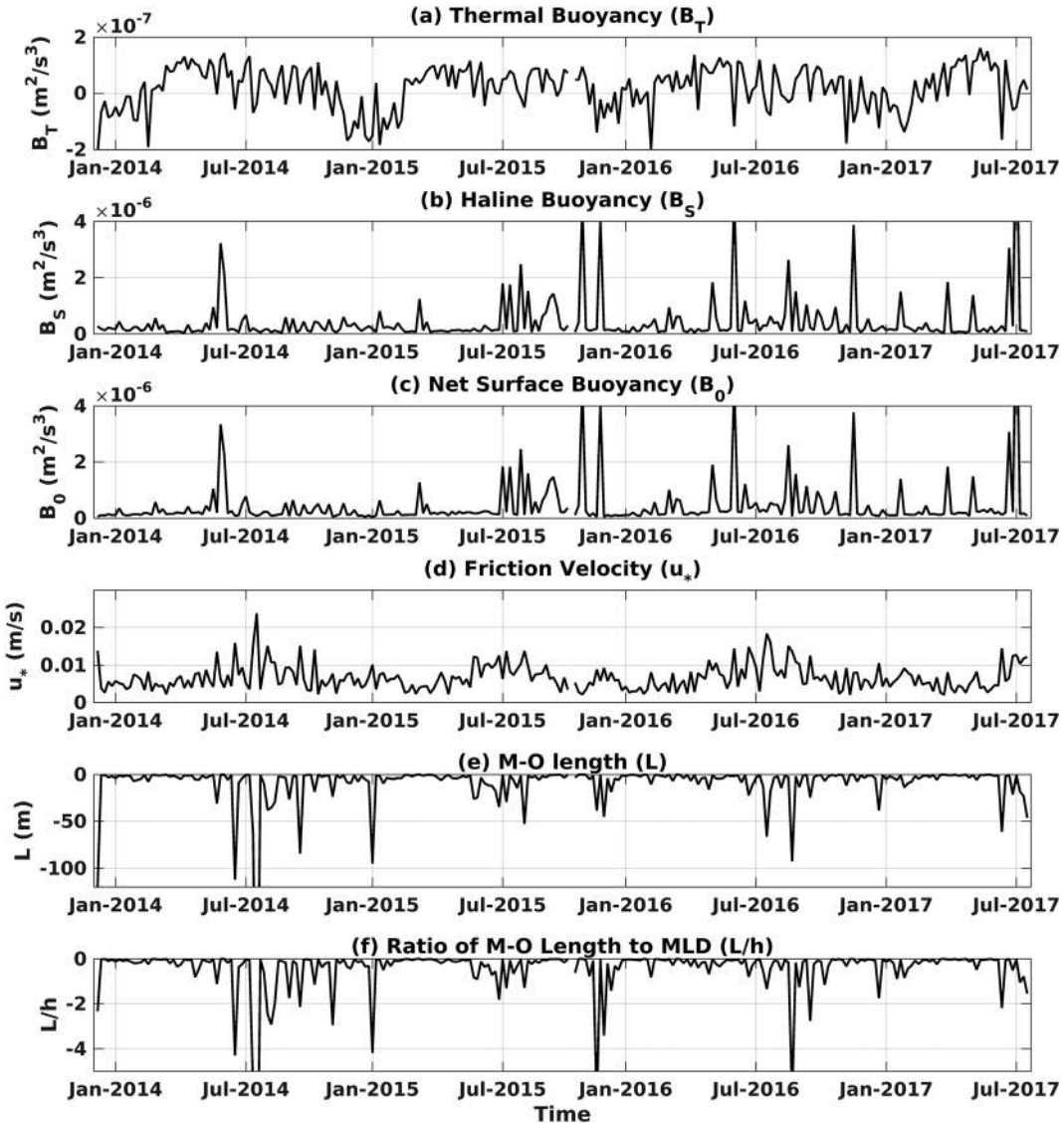

Figure 3. Time series of (a) thermal buoyancy (B_T), (b) haline buoyancy (B_S), (c) net surface buoyancy (B_0), (d) friction velocity (u_*), (e) Monin-Obukhov length (M-O length, L), and (f) ratio of L and the mixed layer depth (h) along the float trajectory.

3.5. Monin-Obukhov Length

The Monin-Obukhov length (M-O length, L) is a measure of the relative importance of the wind forcing to the buoyancy forcing. It is defined as the depth at which turbulence generated by the wind is balanced by the buoyancy. It determines the stability of the water column (AN08; Sutherland et al., 2013). It is negative (positive) for stabilizing (destabilizing) conditions. The M-O length (Figure 3e) in the northern BoB reaches large values (**~50** m) during late summer due to the high WS ($\boldsymbol{u_*}$~0.015 m/s) that is observed from the time series of friction velocity (Figure 3d). During this time very high NSBF limits the M-O length to shallower depths. During the fall and spring, the M-O length is quite small (≤**5** m) due to very low winds ($\boldsymbol{u_*}$<0.01 m/s). In winter, M-O length is less due to loss both buoyancy and wind driven turbulence, except in December when the M-O length is ≥**40** m due to a very small buoyancy flux.

The M-O length (L) is often compared with MLD (h) and their ratio (L/h) is defined as a stability parameter. When $|\boldsymbol{L/h}| > \mathbf{1}$, the ML is dominated by wind mixing. On the other hand, when $|\boldsymbol{L/h}| < \mathbf{1}$, available weak winds are able to mix only the top few meters of the ocean and the balance between wind

energy and thermal buoyancy is achieved at very small depths (AN08). Large $|\boldsymbol{L}/\boldsymbol{h}|$ values indicate dominance of wind mixing over the buoyancy during summer (Figure 3c), which affects the decreasing of MLT. During the spring (thermally stratified) and fall (haline stratified), small L/h indicates the dominance of buoyancy and the ocean gains heat, affecting the MLT to increase. During early winter, large values of $|\boldsymbol{L}/\boldsymbol{h}|$ is due to very small buoyancy, which leads to a deeper ML (Figure 1g) and reduced MLT (Figure 2a). Thus, the M-O length helps to identify the dominance of forcing (wind vs. buoyancy) within the ML. It indirectly affects the change in MLT, which also depends on other factors (see equation (1)).

4. Summary and Conclusions

This study quantifies the thermohaline structure and ML processes through different seasons and is a first-of-its-kind study to establish the seasonality of the hydrography in the northern BoB from long-term observations from a single Argo. The MLHB is investigated to quantify the associated processes. The surface buoyancy flux and the M-O length is calculated to identify the importance of the wind forcing to the buoyancy forcing.

The observed MLD and ILD from the Argo are the deepest during winter. During postmonsoon period (fall), the excess freshwater from precipitation and river runoff generates a BL in the northern BoB, which becomes thick (~80 m) in the winter. The BLT thickens due to the deepening of the ILD because of the downwelling RWs and the heat is trapped at the base of MLD. During winter, the surface cooling (negative NHF tendency) lowers the NST; and thus, the subsurface BL experiences a significant temperature inversion (~2.5°**C**). The ILD decreases to a minimum value, and the BL becomes very thin during spring. During summer, the ILD again starts to increase due to downwelling RWs and BLT reaches up to 40 m with a weak temperature inversion during the late summer monsoon (August). However, in 2015 (a positive IOD year), remote forcing was weak. Therefore, the BLT was comparatively thinner and temperature inversion was absent in 2015. During fall, the MLD is a minimum due to increase in Q_{pen} and decreasing SSS, and a relatively thick (10–20 m) BLT without temperature inversion. Among the four seasons, the ILD largely depends on SSHA and hence with D23 in winter. BLT varies both with ILD and MLD except during spring (Tables S1–S4). The seasonality of the processes is summarized in Table S5.

The roles of BL and temperature inversion on the evolution of MLT can be summarized as follows: The seasonal evolution of the ML shows a deep BL associated with a temperature inversion in the winter as explained above. This temperature inversion diffuses in later winter and distributes heat within the ML in early spring. Come spring, the surface heating begins deep penetration of shortwave radiation through the ML. Hence, it becomes thermally well stratified, resulting in the warmest condition for MLT. During summer, neither thermal inversion (almost nonexistent) nor BL plays any role in dictating the MLT, which is mostly governed by horizontal advection and wind-driven mixing with a high M-O length scale. The range of variation of MLT however becomes limited due to limited shortwave penetration through the clouds. The net surface heat flux picks up in late summer and fall (reduced cloud coverage) to result in higher MLT in a haline-stratified system. Along with freshwater influx, subsequent BL formation happens and MLT drops to its minimum due to heat loss during winter. Temperature inversion starts in middle of winter when surface cooling peaks; and the cycle repeats. Therefore, this analysis indicates that the BL is important in terms of providing extra heat to ML, when the ML deepens due to WS. If there is no BL, the ML deepens due to increasing the wind, then MLT decreases. On the contrary, whenever BL exists, MLT increases (heat available in the BL is more than ML) even if ML deepen. Hence, the existence of BL or Inversion layer, changes the realization of air-sea flux within the ML.

Additionally, we note that the observations from this study will be very valuable for the validation of future ocean models for this region. Preliminary comparison of the observed variability with two ocean models suggests that high vertical resolution and improved mixing scheme are critical needs for better simulation of the ML in the northern BoB. The results of this study clearly point out the need for (i) targeted observations during monsoon and transition periods like fall, (ii) higher-resolution observations near the surface to resolve the relative contribution from buoyancy and wind driving, and (iii) similar analyses in other regions of the global ocean using Argo floats.

Acknowledgments

A. S. and S. S. thank financial support from Space Application Centre (SAC), Indian Space Research Organization (ISRO), Government of India (Grant: SAC/EPSA/4.19/2016). This study was also supported by the first phase of Ministry of Earth Sciences (MoES), Government of India grant to establish a Bay of Bengal Coastal Observatory (BOBCO) at IITBBS (Grant: RP088). Authors acknowledged NCPOR Contribution number J - 03/2019-20 for this work. The authors are grateful to the reviewers and the Editor for constructive suggestions. The figures are generated using Matlab. The data source and availability are given in the Text S1.

References

Anitha, G., Ravichandran, M., & Sayanna, R. (2008). Surface buoyancy flux in Bay of Bengal and Arabian Sea. *Annales Geophysicae*, *26*(3), 395–400. https://doi.org/10.5194/angeo-26-395-2008

Balmaseda, M. A., Mogensen, K., & Weaver, A. T. (2012). Evaluation of the ECMWF ocean reanalysis system ORAS4. *Quarterly Journal of the Royal Meteorological Society*, *139*(674), 1132–1161. https://doi.org/10.1002/qj.2063

Du, Y., Qu, T., Meyers, G., Masumoto, Y., & Sasaki, H. (2005). Seasonal heat budget in the mixed layer of the southeastern tropical Indian Ocean in a high-resolution ocean general circulation model. *Journal of Geophysical Research*, *110*, C04012. https://doi.org/10.1029/2004JC002845

Girishkumar, M. S., Ravichandran, M., & McPhaden, M. J. (2013). Temperature inversions and their influence on the mixed layer heat budget during the winters of 2006-2007 and 2007-2008 in the Bay of Bengal. *Journal of Geophysical Research: Oceans*, *118*, 2426–2437. https://doi.org/10.1002/jgrc.20192

Girishkumar, M. S., Ravichandran, M., McPhaden, M. J., & Rao, R. R. (2011). Intraseasonal variability in barrier layer thickness in the southcentral Bay of Bengal. *Journal of Geophysical Research*, *116*, C03009. https://doi.org/10.1029/2010JC006657

Jana, S., Gangopadhyay, A., & Chakraborty, A. (2015). Impact of seasonal river input on the Bay of Bengal simulation. *Continental Shelf Research*, *104*, 45–62. https://doi.org/10.1016/j.csr.2015.05.001

Johnston, T. M. S., Chaudhuri, D., Mathur, M., Rudnick, D. L., Sengupta, D., Simmons, H. L., et al. (2016). Decay mechanisms of near-inertial mixed layer oscillations in the Bay of Bengal. *Oceanography*, *29*(2), 180–191. https://doi.org/10.5670/oceanog.2016.50

Kara, A. B., Rochford, P. A., & Hurlburt, H. E. (2000). An optimal definition for ocean mixed layer depth. *Journal of Geophysical Research*, *105*(C7), 16,803–16,821. https://doi.org/10.1029/2000JC900072

Kumari, A., Kumar, S. P., & Chakraborty, A. (2018). Seasonal and Interannual variability in the Barrier Layer of the Bay of Bengal. *Journal of Geophysical Research: Oceans*, *123*, 1001–1015. https://doi.org/10.1002/2017JC013213

Millero, F. J., Chen, C. T., Bradshaw, A., & Schleicher, K. (1980). A new high pressure equation of state for seawater. *Deep Sea Research Part A. Oceanographic Research Papers*, *27*(3-4), 255–264. https://doi.org/10.1016/0198-0149(80)90016-3

Montégut, C. B., Vialard, J., Shenoi, S. S., Shankar, D., Durand, F., Ethé, C., & Madec, G. (2007). Simulated seasonal and interannual variability of the mixed layer heat budger in the Northern Indian ocean. *Journal of Climate*, *20*(13), 3249–3268. https://doi.org/10.1175/JCLI4148.1

Parampil, S. R., Gera, A., Ravichandran, M., & Sengupta, D. (2010). Intraseasonal response of mixed layer temperature and salinity in the Bay of Bengal to heat and freshwater flux. *Journal of Geophysical Research*, *115*, C05002. https://doi.org/10.1029/2009JC005790

Paulson, C. A., & Simpson, J. J. (1977). Irradiance Measurements in the Upper Ocean. *Journal of Physical Oceanography*, *7*(6), 952–956. https://doi.org/10.1175/1520-0485(1977)007<0952:IMITUO>2.0.CO;2

Prasad, T. G. (1997). Annual and seasonal mean buoyancy fluxes for the tropical Indian Ocean. *Current Science*, *73*(8), 667–674. https://www.jstor.org/stable/24100427

Praveen Kumar, B., Vialard, J., Lengaigne, M., Murty, V. S. N., & McPhaden, M. J. (2012). TropFlux: air-sea fluxes for the global tropical oceans—Description and evaluation. *Climate Dynamics*, *38*(7-8), 1521–1543. https://doi.org/10.1007/s00382-011-1115-0

Qu, T. (2003). Mixed layer heat balance in the western North Pacific. *Journal of Geophysical Research*, *108*(C7), 3242. https://doi.org/10.1029/2002JC001536

Rao, R. R., Kumar, M. G., Ravichandran, M., Rao, A. R., Gopalakrishna, V. V., & Thadathil, P. (2010). Interannual variability of Kelvin wave propagation in the wave guides of the equatorial Indian Ocean, the coastal Bay of Bengal and the southeastern Arabian Sea during 1993–2006. *Deep Sea Research Part I: Oceanographic Research Papers*, *57*(1), 1–13. https://doi.org/10.1016/j.dsr.2009.10.008

Rao, R. R., & Shivakumar, R. (2003). Seasonal variability of sea surface salinity and salt budget of the mixed layer of the north Indian Ocean. *Journal of Geophysical Research*, *108*(C1), 3009. https://doi.org/10.1029/2001JC000907

Rao, R. R., & Sivakumar, R. (2000). Seasonal variability of near-surface thermal structure and heat budget of the mixed layer of the tropical Indian Ocean from a new global ocean temperature climatology. *Journal of Geophysical Research*, *105*(C1), 995–1015. https://doi.org/10.1029/1999JC900220

Sengupta, D., & Ravichandran, M. (2001). Oscillations of Bay of Bengal sea surface temperature during the 1998 summer monsoon. *Geophysical Research Letters*, *28*(10), 2033–2036. https://doi.org/10.1029/2000GL012548

Sengupta, D., Ray, P. K., & Bhat, G. S. (2002). Spring Warming of the Eastern Arabian Sea and Bay of Bengal from Buoy Data. *Geophysical Research Letters*, *29*(15), 1734. https://doi.org/10.1029/2002GL015340

Shaji, C., Iizuka, S., & Matsuura, T. (2003). Seasonal variability of near-surface heat budget of selected oceanic areas in the North Tropical Indian Ocean. *Journal of Oceanography*, *59*(1), 87–103. https://doi.org/10.1023/A:1022872524758

Shenoi, S. S. C., Shankar, D., & Shetye, S. R. (2002). Differences in heat budgets of the near-surface Arabian Sea and Bay of Bengal: Implications for the summer monsoon. *Journal of Geophysical Research*, *107*(C6), 3052. https://doi.org/10.1029/2000JC000679

Sprintall, J., & Tomczak, M. (1992). Evidence of the barrier layer in the surface layer of the tropics. *Journal of Geophysical Research*, *97*(C5), 7305–7316. https://doi.org/10.1029/92JC00407

Sutherland, G., Ward, B., & Christensen, K. H. (2013). Wave-turbulence scaling in the ocean mixed layer. *Ocean Science*, *9*(4), 597–608. https://doi.org/10.5194/os-9-597-2013

Thadathil, P., Muraleedharan, P. M., Rao, R. R., Somayajulu, Y. K., Reddy, G. V., & Revichandran, C. (2007). Observed seasonal variability of barrier layer in the Bay of Bengal. *Journal of Geophysical Research*, *112*, C02009. https://doi.org/10.1029/2006JC003651

Thompson, B., Gnanaseelan, C., & Salvekar, P. S. (2006). Seasonal evolution of temperature inversions in the north Indian Ocean. *Current Science*, *90*(5), 697–704.

Vinayachandran, P. N., & Shettye, S. R. (1991). The warm pool in the Indian Ocean. *Proceedings of the Indian Academy of Sciences - Earth and Planetary Sciences*, *100*(2), 165–175. https://doi.org/10.1007/BF02839431

Wyrtki, K. (1971). Oceanographic Atlas of the International Indian Ocean Expedition, National Science Foundation Publication, OCE/NSF 86-00-001, 531.

Yu, L. (2003). Variability of the depth of the 20°C isotherm along 6°N in the Bay of Bengal: Its response to remote and local forcing and its relation to satellite SSH variability. *Deep-Sea Research Part II: Topical Studies in Oceanography*, *50*, 2285–2304. https://doi.org/10.1016/S0967-0645(03)00057-2

Yu, L. S., Obrien, J. J., & Yang, J. Y. (1991). On the remote forcing of the circulation in the Bay of Bengal. *Journal of Geophysical Research*, *96*(C11), 20,449–20,454. https://doi.org/10.1029/91JC02424

Zhang, H.-M., & Talley, L. D. (1998). Heat and Buoyancy Budgets and Mixing Rates in the Upper Thermocline of the Indian and Global Oceans. *Journal of Physical Oceanography*, *28*(10), 1961–1978. https://doi.org/10.1175/1520-0485(1998)028<1961:HABBAM>2.0.CO;2